Impedance Characterization of the Transport Properties of Electrolytes Contained within Porous Electrodes and Separators Useful for Li-S Batteries

Rinaldo Raccichini,[a] Liam Furness, James W. Dibden,[b] John R. Owen, and Nuria García-Araez[z]

Department of Chemistry, University of Southampton, Southampton, SO17 1BJ, United Kingdom

Impedance spectroscopy is used to characterize the key transport properties (effective conductivity, MacMullin number, porosity and tortuosity) of electrolyte solutions confined in porous separators and carbon-sulfur composite electrodes useful for application in Li-S batteries. Three relevant electrolyte concentrations, ranging between 1 and 5 molal, are studied. Impedance measurements are performed in symmetrical cells with two identical electrodes, which overcome complications associated with the contributions of the counter-reference electrode. The electrolyte-filled carbon-sulfur composite electrodes can be represented by an "open" Warburg element, modelling the finite-diffusion of ions through the pores coupled to the double-layer charging of the electrode-electrolyte interface. The carbon-sulfur composite electrodes are at a high enough potential (ca. 3 V vs. Li^+/Li) so that charge-transfer reactions of sulfur reduction to polysulfide species are absent during the impedance measurements, and hence capacitive-like behavior is observed at low frequencies. The analysis of the results shows that the rate of transport of ions through porous structures is markedly dependent on the electrode's structure and composition as well as the electrolyte concentration. Synergistic effects, able to enhance the effective conductivity of the electrolyte inside porous composite electrodes, are observed for particular electrode/electrolyte combinations, which are correlated to enhanced performance in Li-S cells.

 [DOI: 10.1149/2.0631811jes]

Manuscript submitted May 22, 2018; revised manuscript received July 23, 2018. Published August 24, 2018.

The future of enhanced electrochemical energy storage systems[1–8] requires significant performance improvements in terms of power and energy density. Achievement of these targets passes through the development of advanced components (e.g., electrolyte, separator and electrode)[9] which requires a better and deeper understanding of the critical properties that lead to enhanced performance.[10–17] This is particularly true in the case of liquid electrolytes used in rechargeable metal-ion (e.g., Li-ion)[18,19] and metal (e.g., Li-S or Al-S)[20–24] batteries.[25,26] It is well known that electrolytes should have high conductivity.[18,27–29] However, as shown in this paper, a high bulk electrolyte conductivity does not guarantee high conductivity of the electrolyte when it infiltrates the porous structures of electrodes and separators. Hence, more advanced methods of analysis are required to understand the effect of the microstructure of the battery components on the macroscopic rate of ion transport.[30–34] Separators have been studied extensively,[35–39] and it is well established that the rate of ion transport depends on the composition, tortuosity, and porosity.[35,40–42] The latter two properties can be correlated using the MacMullin number.[43] However, various studies reported different numerical values for the parameters above, with significant discrepancies in most of the cases.[32,44–50] It is generally accepted that the electrolyte conductivity decreases when the electrolyte is contained within a porous separator,[39] but only in a few cases experimental evidence has been adequately investigated.[32,33,39] In the case of the porous electrodes, the resistance of the electrolyte infiltrated into the electrode is affected by the same structural factors (tortuosity and porosity), which are in turn a function of the electrode composition, method of preparation, and cycling history.[31–33,40,47,51–53] These parameters are particularly relevant in the case of metal-S batteries because a porous carbon matrix is always required in the electrode formulation to facilitate the electrochemical reactions of the active material (i.e., sulfur), which is electrically insulating.

In this work, impedance spectroscopy is used to evaluate the resistance associated with the electrolyte contained in different porous battery components.[54,30–32] Impedance experiments are conventionally carried out in a two-electrode cell set-up where a metal electrode (e.g., lithium) is used as both counter and reference electrode. Then, the impedance of the cell, $Z_{cell}(\omega)$, is given by the sum of the impedance of the working electrode, $Z_{WE}(\omega)$, the impedance of the metal counter-reference electrode, $Z_{CE}(\omega)$, and the impedance (resistance) across the separator, $Z_{sep}(\omega)$,:[30,55–61]

$$Z_{cell}(\omega) = Z_{WE}(\omega) + Z_{CE}(\omega) + Z_{sep}(\omega) \quad [1]$$

Unfortunately, separation of the different components in the overall impedance response is often difficult. Three electrode impedance measurements have been used for the determination of the working electrode impedance, $Z_{WE}(\omega)$,[62–64] but artefacts due to improper cell design are difficult to avoid.[30,33,65–72]

A more convenient approach is to measure the impedance of a cell containing two identical working electrodes (usually called symmetrical cell). Then, the impedance of the cell, $Z_{cell}(\omega)$, is simply two times the impedance of one working electrode, $Z_{WE}(\omega)$, plus the impedance (resistance) of the separator, $Z_{sep}(\omega)$:[30–32,38,39,56,73–78]

$$Z_{cell}(\omega) = 2Z_{WE}(\omega) + Z_{sep}(\omega) \quad [2]$$

This symmetrical cell set-up is adopted in this work to determine the transport properties (e.g., effective conductivity, MacMullin number, tortuosity and porosity) of the electrolyte contained within porous carbon-sulfur composite electrodes. In addition, impedance measurements of symmetrical cells with blocking electrodes are used to determine the transport properties of electrolytes contained within porous separators. We focused our attention on three electrolyte concentrations, useful for Li-S battery applications (i.e., 1.25 molal, 3.5 molal and 5.0 molal), where the salt is lithium bis(trifluoromethanesulfonyl)imide (LiTFSI), and the solvent is 1,3-dioxolane (DOL).[79] Only two previous studies used a symmetrical cell design to investigate the impedance of sulfur-carbon electrodes for Li-S battery applications,[38,74] and, to the best of our knowledge, this is the first study in which a quantitative analysis of the impedance results, by making use of the theory of transport of ions in porous media, is reported for sulfur-carbon composite electrodes.

Experimental

Materials, separators, and electrodes.—Lithium bis(trifluoromethanesulfonyl)imide (LiTFSI) salt (Sigma–Aldrich 99.95% purity) and 1,3-dioxolane (DOL) solvent (Sigma–Aldrich,

[a]Present address: National Physical Laboratory, Hampton Road, Teddington, Middlesex, TW11 0LW, United Kingdom.
[b]Present address: OXIS Energy Ltd. E1 Culham Science Centre, Abingdon OX14 3DB, United Kingdom.
[z]E-mail: N.Garcia-Araez@soton.ac.uk

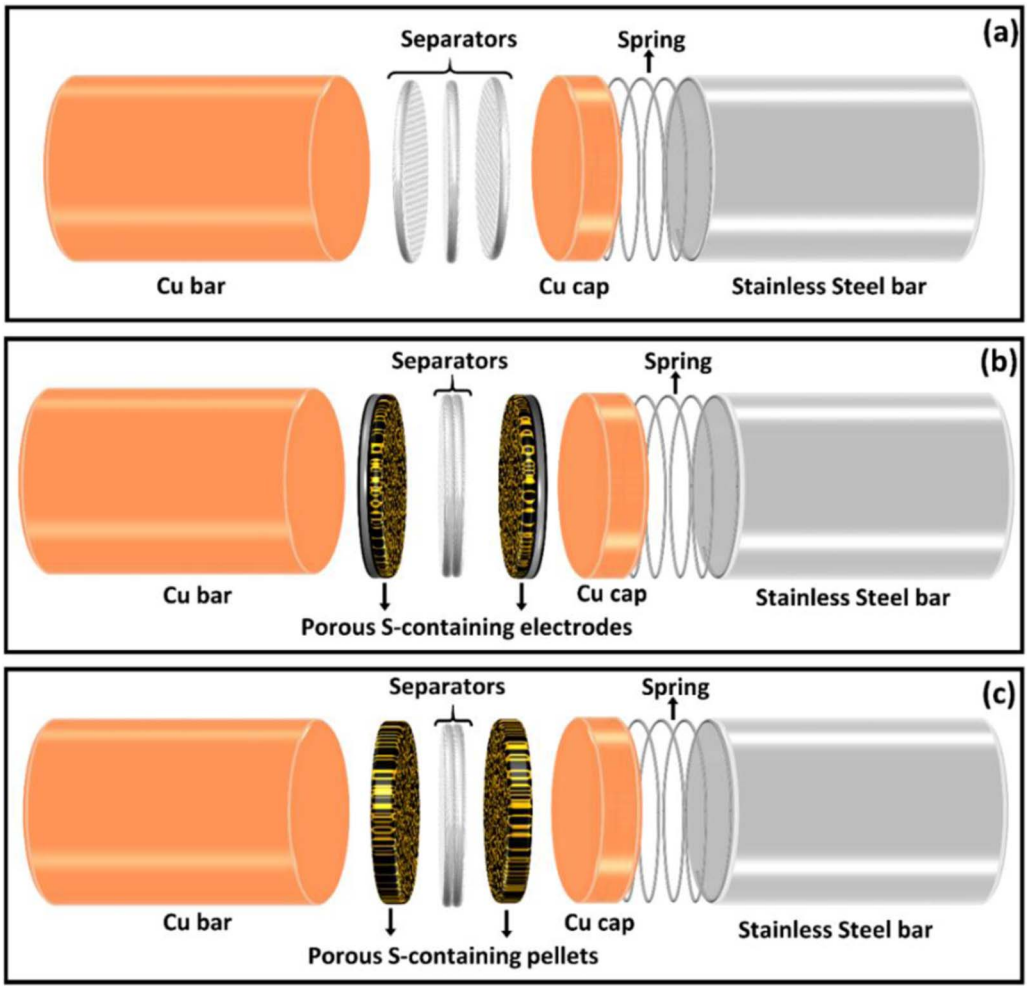

Figure 1. Sketch of the different Swagelok cell set-ups used for the impedance tests of (a) glass-based and olefin-based separators, (b) industrial-scale and (c) laboratory-scale sulfur-containing composite electrodes.

99.8% purity, anhydrous) were used to prepare the electrolyte solutions. LiTFSI was dried for at least 48 hours in a tubular glass vacuum oven (Buchi, pressure < 1 mbar) at 130°C. Electrolytes were prepared inside an Ar-filled glove box (O_2 level < 0.2 ppm and H_2O level < 1.0 ppm) by mixing LiTFSI and DOL with a magnetic stirrer until complete dissolution of the salt. Glass microfiber separator discs (GF/F Whatman, made of borosilicate glass – pore size manufacturer value ≈ 0.7 μm – dry thickness manufacturer value ≈ 420 μm) were cut using a 25 mm, or a 12 mm, diameter arc puncher and dried at 180°C in a glass vacuum oven (Buchi, pressure < 1 mbar) for at least 48 hours. Polyolefin separator discs (V20CFD Toray – pore size < 0.2 μm – dry thickness ≈ 20 μm)[80] were cut using a high–precision 25 mm diameter Nogami handheld puncher and dried at 40°C in a glass vacuum oven (Buchi, pressure < 1 mbar) for at least 48 hours. Industrial-scale produced electrodes with a sulfur content of ≈ 70 wt% and an average sulfur mass loading of ≈ 1.6 mg cm^{-2} were supplied by OXIS Energy Ltd. in forms of large sheets, which were cut using a high–precision 25 mm diameter Nogami handheld puncher. Laboratory-scale produced electrodes were prepared by dry mixing sulfur (sublimed, 100 mesh, Sigma Aldrich, density $= 2.07$ g cm^{-3}), acetylene black (Chevron Phillips Shawinigan Black Acetylene Black, 50% compressed, density $= 1.75$ g cm^{-3}) and polytetrafluoroethylene (Du Pont PTFE fine powder, type 6C-N, density $= 2.14$ g cm^{-3}) in a ground glass mortar for at least 30 minutes. In one preparation, the weight ratio of active material (sulfur), conductive carbon (acetylene black) and binder (PTFE) was 24:66:10, respectively (average sulfur mass loading ≈ 5.0 mg cm^{-2}). In the other preparation, the weight ratio of active material (sulfur), conductive carbon (acetylene black) and binder (PTFE) was 70:20:10, respectively (average sulfur mass loading ≈ 23.4 mg cm^{-2}). The dry mixture was rolled into a sheet (approximately 250 μm) and calendared using a rolling mill (Durston DRM 130) and subsequently cut into pellets (diameter $= 11$ mm) using a single hole punch tool. All the sulfur-containing electrodes were dried at 40°C in a glass vacuum oven (Buchi, pressure < 1 mbar) for at least 24 hours then weighed in air (by means of a METTLER AT261 DeltaRange electronic 5–digit balance, accuracy ± 0.15 mg) and dried again for at least other 8 hours, before transfer to the Ar-filled glove box.

Symmetrical cell assembly and electrochemical test.—Stainless steel Swagelok-type cells (inner diameter 25.4 mm or 12.7 mm) were used with stainless steel bars, metallic copper bars and caps, stainless steel springs, and PTFE or PFA ferrules, as illustrated in Figure 1. Mylar film (thickness $= 0.125$ mm) was used to electrically isolate the body of the cells. To obtain a smooth and oxide-free surface, the copper current collectors were polished using ethanol-filled 1200 grit sandpaper and varying grades of alumina powders (i.e., 25 μm, then 3 μm, then 0.3 μm and finally 0.05 μm). Then, they were cleaned in an ultrasonic bath for at least 20 minutes, dried with Kimtech Science wipes, and transferred to the Ar-filled glove box antechamber where they were dried at room temperature under vacuum for 1 hour. For the characterization of separators, either one, two or three separator layers were incorporated in the cells. 25.4 mm Swagelok cells were used

Table I. Values of porosity (ε_{SEP}) and thickness of the separators.

Separator	ε_{SEP}	Thickness (μm)
GF/F	0.89 ± 0.03 (compressed)	309 ± 30 (compressed)
V20CFD Toray	≈0.43	19 ± 3

to improve the accuracy of the measurements. Each test was carried out using 250 μL/separator of electrolyte solutions and repeated three times for reproducibility. The assembled cells were transferred into a constant climate chamber (Memmert HPP 110, temperature accuracy = 0.1°C; temperature applied = 25°C) and connected to a VMP2 multichannel potentiostat/galvanostat (Biologic) were the impedance spectrum was acquired at the open circuit potential using a perturbation signal of 10 mV in the frequency range 200 kHz – 500 mHz, and fitting of the data was made using the 140 kHz–30 Hz frequency range. After the impedance tests, the cells were disassembled and the thickness of the separators was measured with a thickness gauge.

25.4 mm Swagelok cells were used to study OXIS electrodes and 12.7 mm cells were used for the laboratory-scale electrodes. Two GF/F separator layers were used, and each test was carried out using 250 μL/separator or 63 μL/separator of electrolyte solution for the 25.4 mm or the 12.7 mm cells, respectively. For all the different electrode/electrolyte combinations, the experiments were repeated at least two times for reproducibility. Impedance measurements were done in a frequency range of 30 kHz–20 mHz, and data fitting was done using a 15 kHz–20 mHz frequency range. The rest of experimental procedures were the same as in the case of the characterization of separators.

Porosity and thickness of separators.—The value of porosity (43%) of the V20CFD Toray separator is taken from the manufacturer, and the thickness was measured with a thickness gauge (Mitutoyo ABSOLUTE Digimatic, accuracy ± 3 μm), obtaining a value of 19 μm ± 3 μm, in good agreement with the value of 20 μm reported by the manufacturer.[80,81] In the case of the GF/F Whatman separators, the thickness and porosity of the separator when compressed in the Swagelok cell needed to be determined. Attempts were done to estimate the porosity of the GF/F separators by liquid absorption tests,[35,36,82] but it was difficult to make sure that the excess of liquid was removed from the surface. Therefore, the porosity, ε_{SEP}, was estimated taking into account the weight of the separator:

$$\varepsilon_{SEP} = 1 - \frac{m_{SEP}}{\rho_{glass}\ V_{SEP}} \quad [3]$$

where m_{SEP} is the mass of one separator (38.5 ± 0.2 mg, as determined from the average of 10 separators), ρ_{glass} is the bulk density of the borosilicate glass (2.24 g cm^{-3})[83] and V_{SEP} is the geometric volume of the separator, which was was calculated with:

$$V_{SEP} = \pi\, r_{SEP}^2 t_{SEP} \quad [4]$$

where r_{SEP} and t_{SEP} are the radius (12.5 mm) and thickness (309 ± 30 μm) of the compressed separator. The thickness was measured with a thickness gauge (Mitutoyo ABSOLUTE Digimatic, accuracy ± 3 μm) immediately after disassembly of the cells. The results are summarized in Table I.

Porosity and thickness of electrodes.—Mean values of the porosity of the electrodes (ε_{EL}) were estimated taking into account the density and the weight contents of the bulk materials which compose the electrodes:

$$\varepsilon_{EL} = 1 - \frac{m_{EL}\ \sum_i \left(\frac{\%_i}{100}\ \frac{1}{\rho_i}\right)}{V_{EL}} \quad [5]$$

where m_{EL} is the mass of an individual electrode, $\%_i$ is the weight percentage content of the component i (i.e., sulfur, carbon and binder), ρ_i is the bulk density of the component i, and V_{EL} is the volume of the electrode, which is calculated as follows:

$$V_{EL} = \pi\, r_{EL}^2 t_{EL} \quad [6]$$

where r_{EL} and t_{EL} are the radius and the thickness of the electrode. The calculated values of porosity are reported in Table II. Laboratory-scale produced lithium-sulfur composite electrodes had an average thickness value of about 220 ± 20 μm. The weight percentage of sulfur: carbon: binder and the sulfur mass loading was 24:66:10 and ca. 5.0 mg cm^{-2} in one preparation and 70:20:10 and ca. 23.4 mg cm^{-2} for the other preparation. Details of the OXIS electrode formulation cannot be disclosed.

Table II. Calculated values of porosity (ε_{EL}) for the various electrodes considered in this work.

Electrode	ε_{EL}
OXIS	0.73 ± 0.10
24% S	0.49 ± 0.04
70% S	0.24 ± 0.02

Results and Discussion

Transport properties of electrolytes contained within porous separators.—Figure 2 shows the Nyquist plots of the impedance measurements obtained with either one, two or three layers of electrolyte-filled separators in symmetrical cells containing blocking electrodes.

The impedance of the cell can be described as a combination of a resistance (i.e., R1) and a constant phase element (i.e., CPE) in series[32,84,85] by the following equation:

$$Z_{SEP} = Z_R + 2Z_{CPE} = R1 + \frac{2}{Q_{CPE}(i\omega)^{P_{CPE}}} \quad [7]$$

where $R1$ is the total resistance of all the layers of electrolyte-filled separator, Q_{CPE} is a constant related to the capacitance of the blocking electrodes (which is denoted as T in the Z-view software), ω is the angular frequency and P_{CPE} is the constant phase of the CPE element. In the case of P_{CPE} equal to 1, the Z_{CPE} is equal to the impedance of an ideal capacitor and Q_{CPE} would represents a capacitance. The factor of two multiplying Z_{CPE} in Equation 7 is to account for the fact that the cell contains two copper blocking electrodes. The fit gives values of P_{CPE} between 0.8 – 0.9. If the copper-electrolyte interface behaved as an ideal capacitor with capacitance of 20 μF cm^{-2}, then the capacitance of the cell (equal to $\frac{Q_{CPE}}{2}$) would be expected to be around 5 × 10^{-5} F. The fit gives similar values of $\frac{Q_{CPE}}{2}$ ranging between 2 × 10^{-5} and 9 × 10^{-5} F s$^{P\ -1}$. The values of $R1$ obtained from the fit are summarized in Table III. Each experiment was repeated three times, and the values in Table III are the average values.

In Figure 3, the values of the resistance $R1$ are plotted against the number of separators. The slope of these plots gives the values of the resistance of one separator (i.e., R_{SEP}) (see Table IV) and the intercept provides the amount of the residual resistance (e.g., background contact resistances) associated to the cell set-up (i.e., $R_{SET\text{-}UP}$). In all cases, the resistance of the set-up, $R_{SET\text{-}UP}$, is less than 8% of the resistance of one separator, R_{SEP}, which confirms the reliability of the measurements.

From the values of the resistance per separator (R_{SEP}, see Table IV), the effective ionic conductivity of the electrolyte contained in the separator can be calculated by applying the following general equation:

$$k_{POROUS} = \frac{t}{R_{POROUS} \cdot A} \text{ (for separators : } k_{POROUS} = k_{SEP} \text{ and } R_{POROUS} = R_{SEP}, \text{ for electrodes : } k_{POROUS} = k_{EL} \text{ and } R_{POROUS} = R_{EL}) \quad [8]$$

where t represents the thickness of the separator (when compressed in the cell: 309 ± 30 μm and 19 ± 3 μm for GF/F and Toray,

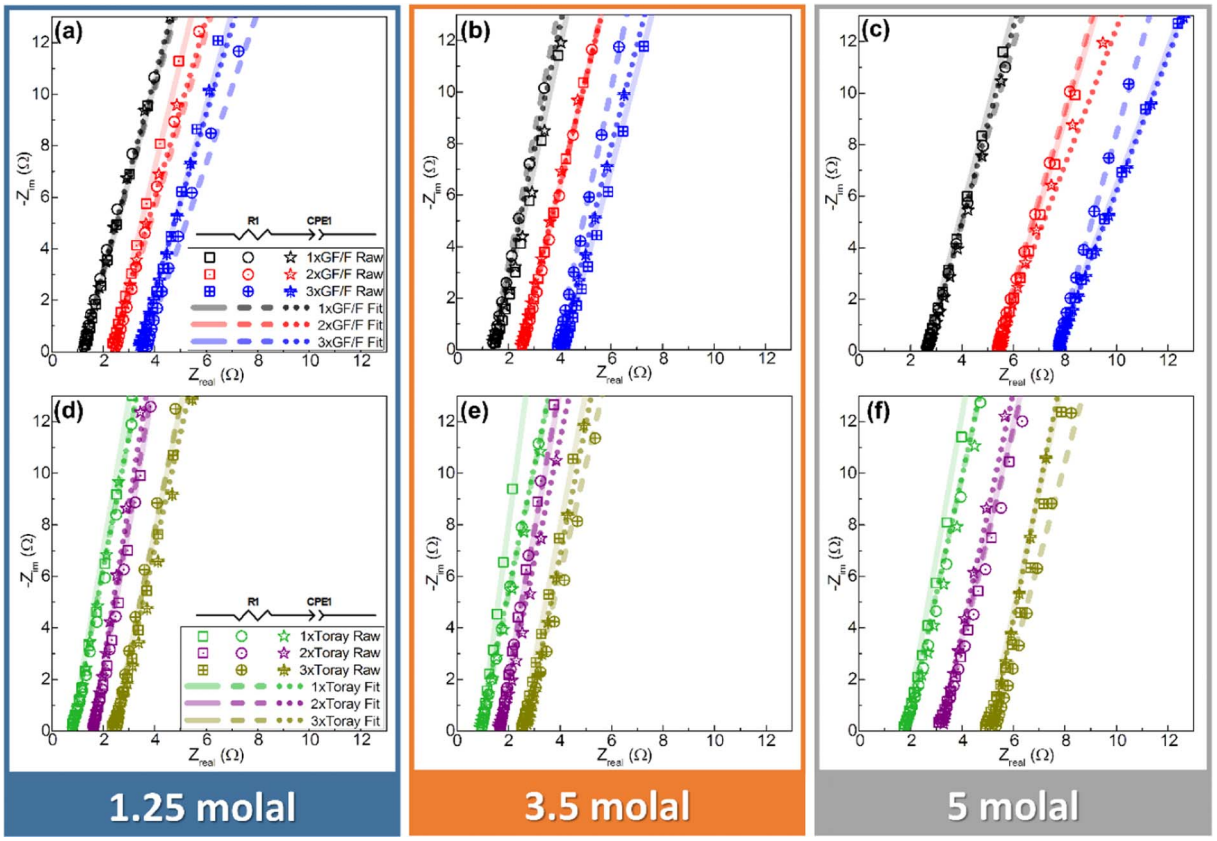

Figure 2. Nyquist plots of the impedance measurements of cells with GF/F separators (a-c) and the Toray separators (d-f) filled with electrolytes of various concentrations. Three independent repeated experiments are shown for each cell.

respectively), and A is the cross-sectional area of the separator. The values of the conductivity of the electrolyte-filled separator (i.e, k_{SEP}) are compared with the bulk electrolyte conductivity values (i.e, k_{BULK}) in Table V. Values of the dynamic viscosity (η) are also reported. The values of k_{BULK} and η were determined in our previous work.[79] Table V shows that, in the case of glass fiber separators, the bulk conductivity is almost entirely retained, while a significant reduction in conductivity is observed in the presence of Toray separators. The main reason for this noticeable dissimilarity is discussed below.

The data reported in Table V shows that the conductivity of the electrolyte-filled separators and the bulk electrolyte conductivity can be significantly different. The relationship between these two quantities is given by the MacMullin number (N_M). In general, the MacMullin number describes the effect of a porous microstructure on the macroscopic transport properties of the electrolyte,[43] and it can be defined as follows:[32,44,45,47,50]

$$N_M = \frac{k_{BULK}}{k_{POROUS}} \quad [9a]$$

$$N_M = \frac{\tau}{\varepsilon} \quad [9b]$$

Equation 9a is used here to calculate the numerical values of N_M, which we call $N_{M,SEP}$ for separators and $N_{M,EL}$ for electrodes. Then, Equation 9b is used to evaluate the effective tortuosity, τ, taking into account the values of porosity ε of the separators (and latter, of the electrodes) reported in Table I (and Table II for the electrodes). The calculated values of $N_{M,SEP}$ and τ_{SEP} are reported in Table VI.

Table VI shows that the MacMullin numbers, $N_{M,SEP}$, of the glass fiber separator are close to one in all cases, while in the case of the Toray separator, the values are much higher. This is because, in the latter, the conductivity retention is much poorer. This is due, in part, to the lower porosity of Toray separator (ca. 43%),[80] as compared to the glass fiber separator (ca 89%). However, the main reason is the much higher tortuosity of the Toray separator, as shown in Table VI. The effective tortuosity can be understood as the increase in the path-length of ion transport (in the simplest definition, tortuosity is simply the ratio of the effective ion pathlength and the geometric thickness of the porous material). The definition of effective tortuosity in Equation 9b is an empirical definition that can include more complex effects such as pore clogging and pore narrowing.[32,44–50] For the glass fiber separator, values of tortuosity are found to be close to unity, evidencing facile transport and good wetting of the whole porous structure. Previous studies using ionic-liquids have also reported MacMullin number for glass fiber separators very close to unity.[41] The results of the MacMullin number and effective tortuosiy of the Toray separator are also in good agreement with those reported in the literature for similar types of polyolefin separators.[32,41,86–88] Table VI also shows

Table III. Summary of the R1 values obtained from the fit of the impedance data in Figure 2 using Equation 7.

Separator n°	Molality (mole LiTFSI/kg DOL)	R1 (Ω) GF/F	R1 (Ω) Toray
1	1.25	1.19 ± 0.04	0.82 ± 0.02
	3.5	1.43 ± 0.06	0.92 ± 0.03
	5	2.65 ± 0.06	1.84 ± 0.03
2	1.25	2.34 ± 0.05	1.62 ± 0.01
	3.5	2.49 ± 0.05	1.64 ± 0.01
	5	5.34 ± 0.05	3.20 ± 0.04
3	1.25	3.44 ± 0.11	2.44 ± 0.02
	3.5	4.03 ± 0.15	2.60 ± 0.08
	5	7.67 ± 0.04	5.15 ± 0.10

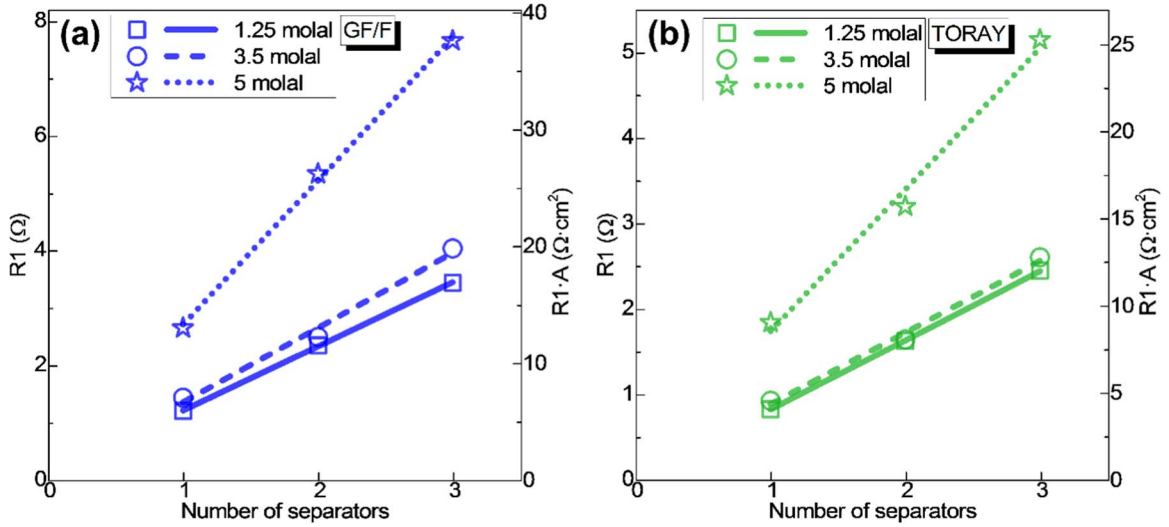

Figure 3. Plot of the R1 values in Table III against the number of separators in the cell, for GF/F (a) and Toray (b) separators filled with different electrolyte concentrations. The straight lines are the linear fit.

that the MacMullin number and the effective tortuosity vary little with the electrolyte concentration, even for the more concentrated solution (which are highly viscous). This suggests that poor wetting of the separators (due to trapped gas bubbles as a result of improper cell degassing, for example) is not an issue, confirming the suitability of highly concentrated solutions (e.g., solvent-in-salt electrolytes) for practical Li-S cells.

Transport properties of electrolytes contained within porous electrodes.—The impedance spectra of the porous carbon-sulfur composite electrodes in symmetrical cell configuration are shown in Figures 4a–4c, for the various electrolyte concentrations. The impedance values have been normalized by the cross-sectional areas of the electrodes (4.9 cm^2 for the OXIS electrodes and 0.95 cm^2 for the laboratory-scale electrodes). The impedance spectra in Figure 4 do not show any contribution due to the reduction of sulfur into polysulfide species. This is because the potential of the as-prepared carbon-sulfur electrodes is high enough (i.e., ca. 3 V when measured vs. Li^+/Li in Li-S cells containing an Ohara glass separator that stops shuttling of sulfur species to the Li electrode),[89] so that the small potential perturbation associated to the impedance measurements does not trigger any charge transfer reactions of sulfur reduction to polysulfides. As a result, the electrochemical response of the electrodes at low frequencies is dominated by double-layer charging of the electrode-electrolyte interface (i.e., capacitive or blocking behavior). In other words, at the open circuit potential, the charge-transfer resistance of

Table VI. Calculated values of the MacMullin number ($N_{M,SEP}$) and effective tortuosity (τ_{SEP}) for the various electrolyte/separator combinations. The calculations have been done using the values of porosity (ε_{SEP}) in Table I and the bulk conductivity (k_{BULK}) and the conductivity of the electrolyte-filled separator (k_{SEP}) in Table V.

Molality	$N_{M,SEP}$		τ_{SEP}	
(mole LiTFSI/kg DOL)	GF/F	Toray	GF/F	Toray
1.25	1.0 ± 0.1	11.7 ± 1.9	0.9 ± 0.1	5.1 ± 0.8
3.5	1.2 ± 0.2	13.2 ± 2.1	1.1 ± 0.1	5.7 ± 0.9
5	1.3 ± 0.1	14.6 ± 2.7	1.2 ± 0.1	6.2 ± 1.0

Table IV. Values of the resistance per separator (R_{SEP}), as obtained from the slope of the linear fit in Figure 3. The table also shows the values of the residual resistance of the cell ($R_{SET\text{-}UP}$), as obtained from the intercept of the fit in Figure 3.

	R_{SEP}				$R_{SET\text{-}UP}$			
	GF/F		Toray		GF/F		Toray	
Molality (mole LiTFSI/kg DOL)	(Ω)	(Ω · cm^2)	(Ω)	(Ω · cm^2)	(Ω)	(Ω · cm^2)	(Ω)	(Ω · cm^2)
1.25	1.12 ± 0.02	5.52 ± 0.10	0.81 ± 0.01	3.98 ± 0.05	0.08 ± 0.03	0.40 ± 0.15	0.01 ± 0.01	0.05 ± 0.05
3.5	1.30 ± 0.14	6.38 ± 0.69	0.84 ± 0.07	4.12 ± 0.34	0.05 ± 0.10	0.25 ± 0.50	0.04 ± 0.05	0.20 ± 0.25
5	2.51 ± 0.11	12.31 ± 0.54	1.66 ± 0.17	8.15 ± 0.83	0.20 ± 0.15	0.98 ± 0.75	0.08 ± 0.10	0.39 ± 0.49

Table V. Conductivity values of electrolyte-filled separators (k_{SEP}). For comparison, the table also shows the bulk electrolyte conductivity (k_{BULK}) and the bulk electrolyte dynamic viscosity (η), as obtained in Reference 79.

			k_{SEP} (mS cm^{-1})	
Molality (mole LiTFSI/kg DOL)	η[79] (mPoise)	k_{BULK}[79] (mS cm^{-1})	GF/F	Toray
1.25	16.8	5.63	5.60 ± 0.54	0.48 ± 0.08
3.5	99.9	6.06	4.84 ± 0.70	0.46 ± 0.07
5	303.0	3.37	2.51 ± 0.24	0.23 ± 0.04

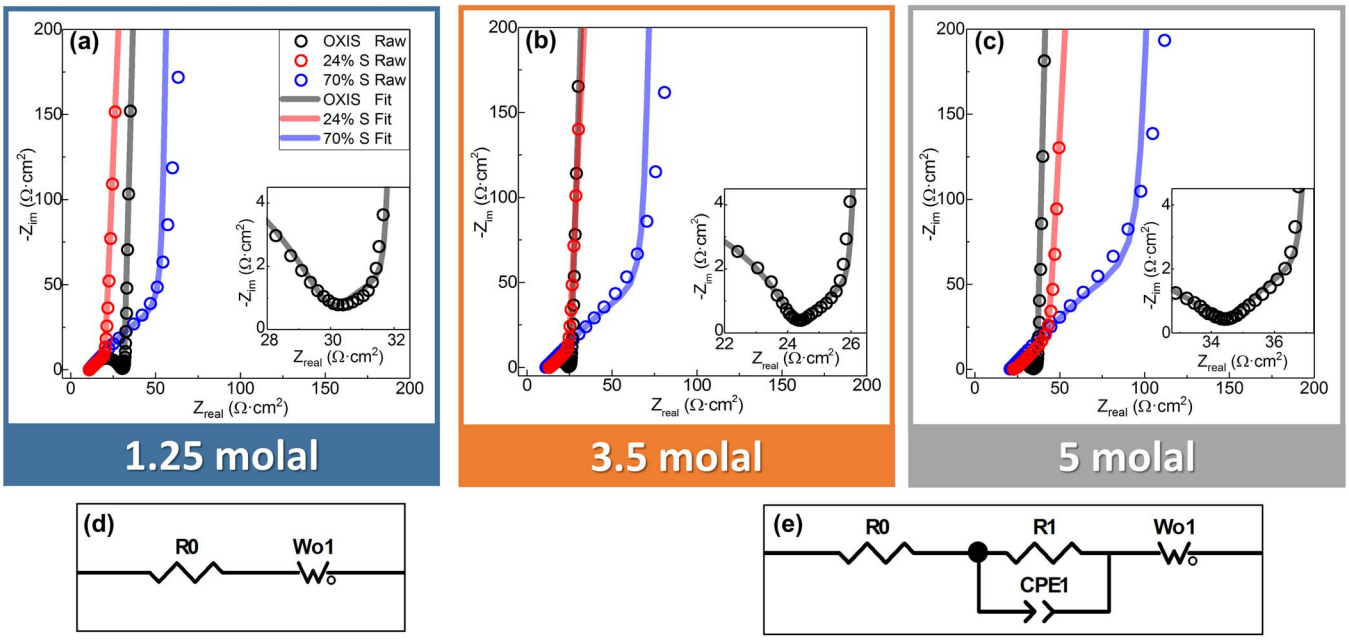

Figure 4. (a-c) Nyquist plots of electrolyte-filled carbon-sulfur composite electrodes in symmetrical cell configuration. The insets show a zoom-in of the plot for the OXIS electrodes; (d) equivalent circuit used to fit the data of the laboratory-scale produced electrodes; (e) equivalent circuit used to fit the data of the OXIS electrodes.

sulfur reduction to polysulfides is high enough so that the reaction does not affect the impedance measurements. This is in agreement with previous impedance studies with carbon-sulfur composite electrodes in symmetrical cells, which showed that replacement of sulfur by inert Al_2O_3 particles produced very similar impedance results, hence demonstrating the absence of charge-transfer reactions.[38,74]

The impedance behavior of the porous electrodes in the whole frequency range can be described by an equivalent circuit model defined as "transmission line model" as proposed by Robert De Levie.[90–92] This model takes into account: (i) the fine-length diffusion of ions contained within the pores of the electrolyte-filled electrode, (ii) the transport of electrons through the carbon conductive matrix of the composite electrode, and (iii) the charging of the carbon-electrolyte interface as a double-layer capacitor, which in our case is modelled as a constant phase element to include deviations from ideal capacitive behavior.[30–32,84,85,93–95] The electrical component associated to the "transmission line model" is called "open" Warburg element (i.e., Wo) which can be described by the following equation:

$$Z_{Wo} = R_{W_o} \frac{coth\left(\left[T_{W_o} i\omega\right]^{P_{Wo}}\right)}{\left(T_{W_o} i\omega\right)^{P_{Wo}}} \qquad [10]$$

where R_{W_o} represents the sum of all the resistances associated with the electrolyte contained within the porous electrode, T_{W_o} is a characteristic time constant and P_{Wo} is an exponent associated to deviations from non-ideal capacitive behavior (for ideal behavior $P_{Wo} = 0.5$). Thus, the impedance of the cells with the laboratory-scale produced porous electrodes (i.e., the 24% S and the 70% S pellets) can be described by the following equation:

$$Z_{PELLET} = Z_{R0} + 2Z_{Wo1} = R0 + 2R_{W_{o1}} \frac{coth\left(\left[T_{W_{o1}} i\omega\right]^{P_{Wo1}}\right)}{\left(T_{W_{o1}} i\omega\right)^{P_{Wo1}}} \qquad [11]$$

where $R0$ is the resistance of the separator (in this case, two electrolyte-filled glass fiber separators) and R_{Wo1} is the resistance of a single electrolyte-filled porous electrode. The factor of two multiplying Z_{Wo1} in Equation 11 accounts for the fact that two identical electrodes have been used in the symmetrical cell set-up. Figure 4 shows that the model fits the experimental data very well. The impedance spectra of the cells with the industrial-scale produced electrodes (black dots and lines in Figures 4a–4c) contain an additional depressed semicircle. This semicircle has been ascribed to the contact resistance of the aluminum current collector and the composite electrode.[32,33,96,97] In agreement with previous studies, we only observed the depressed semicircle with aluminum or unpolished copper current collectors (data not shown here), which indicates that it is due to the presence of an oxide layer. The depressed semicircle can be described as a contact resistance (i.e., $R1$) and a constant phase element (i.e., $CPE1$) in parallel, and the whole impedance data of the cell can be fitted with the following equation:

$$\begin{aligned} Z_{OXIS} &= Z_{R0} + \left(\frac{2}{\frac{1}{Z_{R1}} + \frac{1}{Z_{CPE1}}}\right) + 2Z_{Wo1} \\ &= R0 + \left(\frac{2}{\frac{1}{R1} + \frac{1}{1/\left[Q_{CPE1}(i\omega)^{P_{CPE1}}\right]}}\right) \\ &\quad + 2R_{W_{o1}} \frac{coth\left(\left[T_{W_{o1}} i\omega\right]^{P_{Wo1}}\right)}{\left(T_{W_{o1}} i\omega\right)^{P_{Wo1}}} \end{aligned} \qquad [12]$$

where Z_{Wo1} is the impedance of one electrolyte-infiltrated porous electrode, which can be described with an open Warburg element, as discussed above. The insets in Figure 4 show a zoom-in of the impedance results showing the characteristic behavior of the open Warburg element. Figures 4d–4e show the equivalent circuits used to fit the data. The results of the fit are summarized in Table VII.

Table VII shows that $R_{W_{o1}}$ (that is, the resistance of the electrolyte contained inside one porous electrode of unity area 1 cm^2) is much smaller for the OXIS electrodes than for the laboratory-scale produced pellets, and for the latter, increasing the sulfur content increases the value of $R_{W_{o1}}$. Similarly, the value of $T_{W_{o1}}$ (that is, the

Table VII. Values of the total resistance (R_{Wo1}), time constant (T_{Wo1}) and exponent (P_{Wo1}) associated to the open Warburg element of the fit of the impedance data in Figure 4 to Equation 11 for the laboratory-scale electrodes, and to Equation 12 for the OXIS electrodes.

Molality (mole LiTFSI/kg DOL)	Wo1 Fit								
	R_{Wo1} ($\Omega \cdot cm^2$)			T_{Wo1} (ms)			P_{Wo1}		
	OXIS	24% S	70% S	OXIS	24% S	70% S	OXIS	24% S	70% S
1.25	2.91 ± 0.03	14.7 ± 1.1	62 ± 4	24.4 ± 0.4	631 ± 91	1175 ± 76	0.490 ± 0.002	0.488 ± 0.001	0.494 ± 0.001
3.5	2.71 ± 0.02	16.9± 0.2	89 ± 4	21.6 ± 0.3	715 ± 18	1870 ± 118	0.491 ± 0.001	0.485 ± 0.001	0.493 ± 0.001
5	3.88 ± 0.05	29.1± 1.45	113 ± 7	28.0 ± 0.9	1333 ± 137	2199 ± 121	0.491 ± 0.001	0.485 ± 0.001	0.488 ± 0.01

Table VIII. Conductivity of the electrolyte contained within the various sulfur-carbon composite electrodes (k_{EL}). For comparison, the bulk electrolyte conductivity (k_{BULK}) is also included, as reported in Reference 79.

Molality (mole LiTFSI/kg DOL)	k_{BULK}[79] (mS cm^{-1})	k_{EL} (mS cm^{-1})		
		OXIS	24% S	70% S
1.25	5.63	1.48 ± 0.21	1.50 ± 0.18	0.35 ± 0.03
3.5	6.06	1.59 ± 0.22	1.30 ± 0.12	0.25 ± 0.02
5	3.37	1.11 ± 0.15	0.76 ± 0.07	0.19 ± 0.02

time required for ions to penetrate the whole porous electrode) is also significantly shorter for the OXIS electrodes. Those results are, in part, due to the thinner thickness of the OXIS electrodes. Thus, the values of $R_{W_{o1}}$ are used to calculate the effective conductivity of the electrolyte contained within the different electrodes, k_{EL}, which is obtained using Equation 8, taking into account that $k_{EL} = k_{POROUS}$, t is the electrode thickness, and $R_{POROUS} = R_{EL} = R_{Wo1}/A$, where A is the geometrical area of the electrode. The results are shown in Table VIII.

The MacMullin number of the electrolyte-filled electrodes, $N_{M,\,EL}$, can be obtained from the ratio of the effective conductivity in the porous media (i.e., $k_{POROUS} = k_{EL}$ in this case) and in the bulk (i.e., k_{BULK}), as shown in Equation 9a. In addition, using Equation 9b, the effective tortuosity of the electrodes, τ_{EL}, can be obtained by using the values of the electrodes porosity ε_{EL} described in Table II. The results are summarized in Table IX.

To summarize, Figure 5 illustrates the different scenarios studied and assessed in this work. The resistance of the electrolyte confined inside one electrode of unity area (R_{Wo1}, Table VII) is found to be minimum for the combination of OXIS electrodes with 3.5 molal electrolyte. Interestingly, this particular combination was reported to lead to improved performance (capacity retention) in Li-S cells.[98] For the laboratory-scale electrodes, the resistance increases markedly with increasing the sulfur content (Table VII), and it is also found that the resistance increases with increasing the electrolyte concentration (Table VII), which can be attributed to the increase in the bulk electrolyte viscosity (Table V). However, Table VIII shows that the variation of the effective conductivity of the electrolyte inside the composite electrodes (k_{EL}, as calculated from the resistance values) does not exactly follow the bulk electrolyte conductivity, k_{BULK}, and higher values of the MacMullin number are observed at 3.5 molal concentration than at other concentrations ($N_{M,\,EL}$, Table IX). This is reflected in a higher effective tortuosity (τ_{EL}. Table IX), which could be attributed to poorer electrode-electrolyte interactions for that particular combination. The results of the effective tortuosity (τ_{EL}, Table IX) clearly show that increasing the sulfur content of the laboratory-scale composite electrodes produces a marked increase in the tortuosity. This can be attributed to the fact that sulfur is soft and hence facilitates blocking of the carbon pores, which results in an increase of the effective pathlength for ion transport. However, Table IX also shows that for advanced electrode formulations, such as those of the OXIS electrodes, very low values of the effective tortuosity can be achieved at very high sulfur loadings (of 70%). This demonstrates that the effective tortuosity (and other key transport properties) will critically depend on the details of electrode formulation, including the physico-chemical properties of carbon, method of impregnation of sulfur, method of electrode preparation, binder, etc. and the present study shows that electrode and electrolyte optimization has to be done synergistically.

Conclusions

We have shown that the analysis of impedance measurements of porous separators and porous carbon-sulfur composite electrodes allows the evaluation of: (i) the resistance of the electrolyte when confined within the porous structure, (ii) the effective conductivity, (iii) the MacMullin number, and (iv) the effective tortuosity. The resistance of the electrolyte contained within the porous structures of the separator and electrode represents a measure of the rate of transport of Li^+ ions contained within those battery components. The reduction of sulfur to Li_2S requires Li^+ ions, and hence fast

Table IX. Calculated values of the MacMullin number ($N_{M,EL}$) and effective tortuosity (τ_{EL}) for the various electrolyte/electrode combinations. The calculations have been done using the values of porosity (ε_{EL}) in Table II and the bulk conductivity (k_{BULK}) and the conductivity of the electrolyte-filled electrode (k_{SEP}) in Table VIII.

Molality (mole LiTFSI/kg DOL)	$N_{M,EL}$			τ_{EL}		
	OXIS	24% S	70% S	OXIS	24% S	70% S
1.25	3.8 ± 0.5	3.7 ± 0.4	15.9 ± 1.8	2.8 ± 0.4	1.8 ± 0.2	3.8 ± 0.4
3.5	3.8 ± 0.5	4.7 ± 0.4	24.4 ± 2.5	2.8 ± 0.4	2.3 ± 0.2	5.9 ± 0.5
5	3.0 ± 0.4	4.5 ± 0.5	17.4 ± 1.9	2.2 ± 0.3	2.2 ± 0.2	4.2 ± 0.4

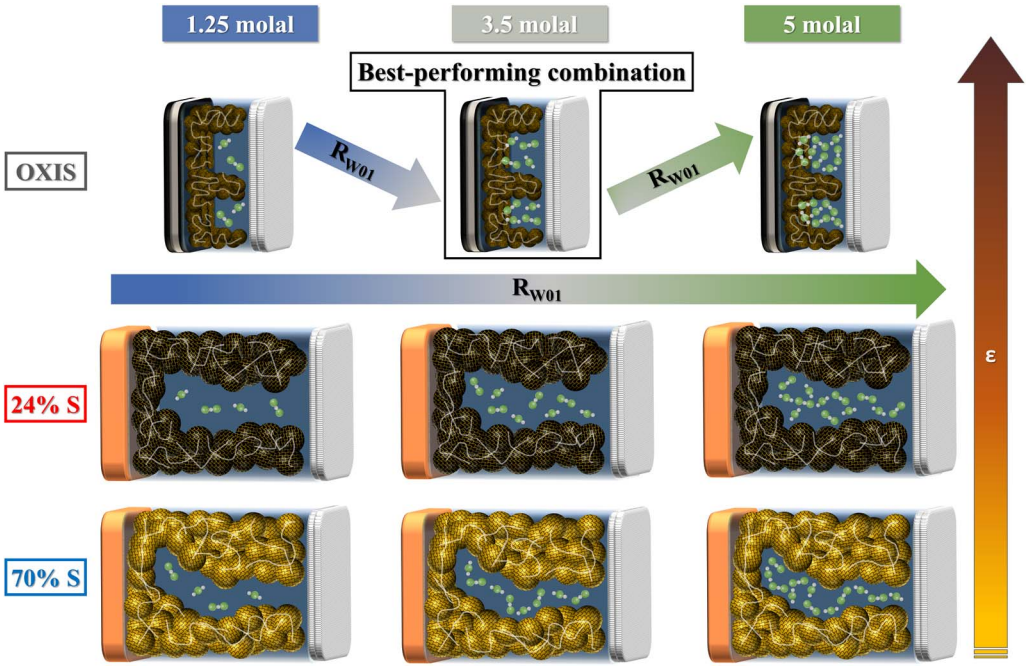

Figure 5. Schematic representation of the cross-section of a Swagelok cell for various electrode/electrolyte combinations. The sulfur-carbon active materials is represented by the black/yellow spheres. The binder is represented by the gray curve line. The electrolyte solution is represented by the transparent blue background (i.e., the solvent DOL) and the grey/green balls (which represent the various ion associations of the LiTFSI salt). The current collectors and the separators show the same colors already reported in Figure 1.

enough supply of Li^+ ions is required for optimal operation of the cell. Extensive work has been done to develop carbon-sulfur composite electrode structures that prevent polysulfide diffusion away from the electrode,[13,21,99–103] but fast enough transport of polysulfides within and to the whole electrode structure is necessary to assure full utilization of sulfur[104–107] and to avoid buildup of high local concentrations of polysulfides, since the latter will lead to precipitation of Li_2S and/or sulfur[108,109] and consequent pore clogging.[110] Thus, an optimal value of the rate of ion transport is expected to lead to optimized performance, and this work describes an approach to quantify it.

Acknowledgments

This work was supported by OXIS Energy Ltd., the Engineering and Physical Sciences Research Council (EPSRC), Innovate UK, and the University of Southampton under the project "Microgrid Energy Storage Using Lithium Sulfur Batteries (MESS)" (EP/P019099/1). R.R and N.G.A. also acknowledge support from the European Commission through the FET-OPEN project "Sulfur-Aluminum Battery with Advanced Polymeric Gel Electrolytes" SALBAGE project (Project ID: 766581). L.F. acknowledges OXIS Energy Ltd., the University of Southampton, and EPSRC (EP/M508147/1) for a doctoral studentship. J.W.D. acknowledges OXIS Energy Ltd. and, the University of Southampton and EPSRC (EP/M50662X/1) for a CASE studentship. N.G.A. acknowledges EPSRC (EP/N024303/1) for an early career fellowship. Last but not least, the authors thank Ashley Brew, Ashley Cooke, Lisset Urrutia, David Ainsworth, and Tom Cleaver of OXIS Energy Ltd. for the productive scientific discussions. Georgia Cooke is also gratefully acknowledged for the preliminary experiments carried out during her undergraduate project. The data for this article are available from the University of Southampton at DOI: https://doi.org/10.5258/SOTON/D0586

List of Symbols

A	Cross-sectional area	cm^2
k_{BULK}	Bulk electrolyte conductivity	$S\ cm^{-1}$
k_{POROUS}	effective electrolyte conductivity in a porous medium	$S\ cm^{-1}$
N_M	MacMullin number	-
P_{CPE}	CPE phase	-
P_{W0}	Open Warburg phase	-
Q_{CPE}	CPE capacitance	$F\ s^{P-1}$
r	radius	cm
R	resistance	Ω
R_{W0}	Open Warburg time resistance	Ω
t	thickness	cm
T_{W0}	Open Warburg time constant	s
V	volume	cm^3
W	weight	g
Z	complex impedance	Ω
	Greek	
ω	angular frequency	s^{-1}
ε	porosity	-
ρ	density	$g\ cm^{-3}$
η	Dynamic viscosity	Poise
τ	Effective tortuosity	-

ORCID

Rinaldo Raccichini https://orcid.org/0000-0003-1507-2739
John R. Owen https://orcid.org/0000-0002-4938-3693
Nuria García-Araez https://orcid.org/0000-0001-9095-2379

References

1. J. R. Owen, *Chem. Soc. Rev.*, **26**, 259 (1997).
2. J. Muldoon, C. B. Bucur, and T. Gregory, *Chem. Rev.*, **114**, 11683 (2014).
3. N. S. Choi et al., *Angew. Chemie - Int. Ed.*, **51**, 9994 (2012).

4. M. M. Thackeray, C. Wolverton, and E. D. Isaacs, *Energy Environ. Sci.*, **5**, 7854 (2012).
5. J.-M. Tarascon and M. Armand, *Nature*, **414**, 359 (2001).
6. J. B. Goodenough and K.-S. Park, *J. Am. Chem. Soc.*, **135**, 1167 (2013).
7. M. Armand and J.-M. Tarascon, *Nature*, **451**, 652 (2008).
8. D. Larcher and J. Tarascon, *Nat. Chem.*, **7**, 19 (2014).
9. M. Winter and R. J. Brodd, *Chem. Rev.*, **104**, 4245 (2004).
10. C. P. Grey and J. M. Tarascon, *Nat. Mater.*, **16**, 45 (2016).
11. M. R. Palacín and A. De Guibert, *Science*, **351**, 1253292 (2016).
12. M. Wild et al., *Energy Environ. Sci.*, **8**, 3477 (2015).
13. S. Urbonaite, T. Poux, and P. Novák, *Adv. Energy Mater.*, **5**, 1 (2015).
14. J. Gao and H. D. Abruña, *J. Phys. Chem. Lett.*, **5**, 882 (2014).
15. B. D. McCloskey, *J. Phys. Chem. Lett.*, **6**, 4581 (2015).
16. T. Cleaver, P. Kovacik, M. Marinescu, T. Zhang, and G. Offer, *J. Electrochem. Soc.*, **165**, A6029 (2018).
17. C. Li et al., *J. Power Sources*, **326**, 1 (2016).
18. K. Xu, *Chem. Rev.*, **104**, 4303 (2004).
19. M. Roberts et al., *J. Mater. Chem.*, **21**, 9876 (2011).
20. M. Barghamadi et al., *Energy Environ. Sci.*, **7**, 3902 (2014).
21. A. Manthiram, Y. Fu, S. Chung, C. Zu, and Y. Su, *Chem. Rev.*, **114**, 11751 (2014).
22. S. Zhang, K. Ueno, K. Dokko, and M. Watanabe, *Adv. Energy Mater.*, **5**, 1500117 (2015).
23. G. A. Elia et al., *Adv. Mater.*, **28**, 7564 (2016).
24. J. W. Dibden, N. Meddings, J. R. Owen, and N. Garcia-Araez, *ChemElectroChem*, **5**, 445 (2018).
25. K. Xu, *Chem. Rev.*, **114**, 11503 (2014).
26. G. A. Giffin, *J. Mater. Chem. A*, **4**, 13378 (2016).
27. Y. Yamada and A. Yamada, *J. Electrochem. Soc.*, **162**, A2406 (2015).
28. A. Varzi, R. Raccichini, S. Passerini, and B. Scrosati, *J. Mater. Chem. A*, **4**, 17251 (2016).
29. A. Manthiram, X. Yu, and S. Wang, *Nat. Rev. Mater.*, **2**, 16103 (2017).
30. N. Ogihara et al., *J. Electrochem. Soc.*, **159**, A1034 (2012).
31. N. Ogihara, Y. Itou, T. Sasaki, and Y. Takeuchi, *J. Phys. Chem. C*, **119**, 4612 (2015).
32. J. Landesfeind, J. Hattendorff, A. Ehrl, W. A. Wall, and H. A. Gasteiger, *J. Electrochem. Soc.*, **163**, A1373 (2016).
33. J. Landesfeind, D. Pritzl, and H. A. Gasteiger, *J. Electrochem. Soc.*, **164**, A1773 (2017).
34. D. W. Abarbanel, K. J. Nelson, and J. R. Dahn, *J. Electrochem. Soc.*, **163**, A522 (2016).
35. P. Arora and Z. (John) Zhang, *Chem. Rev.*, **104**, 4419 (2004).
36. V. Deimede and C. Elmasides, *Energy Technol.*, **3**, 453 (2015).
37. Y. Xiang et al., *ChemSusChem*, **9**, 3023 (2016).
38. J. Conder et al., *Electrochim. Acta*, **244**, 61 (2017).
39. J. Conder et al., *Electrochim. Acta*, **255**, 379 (2017).
40. B. Tjaden, D. J. L. Brett, and P. R. Shearing, *Int. Mater. Rev.*, **63**, 47 (2018).
41. M. Kirchhöfer, J. Von Zamory, E. Paillard, and S. Passerini, *Int. J. Mol. Sci.*, **15**, 14868 (2014).
42. W. Zhang et al., *Small*, **14**, 1 (2018).
43. R. B. MacMullin and G. A. Muccini, *AIChE J.*, **2** (1956).
44. I. V. Thorat et al., *J. Power Sources*, **188**, 592 (2009).
45. M. Doyle and J. Newman, *J. Electrochem. Soc.*, **143**, 1890 (1996).
46. D. Fan and R. E. White, *J. Electrochem. Soc.*, **138**, 17 (1991).
47. D. Kehrwald, P. R. Shearing, N. P. Brandon, P. K. Sinha, and S. J. Harris, *J. Electrochem. Soc.*, **158**, A1393 (2011).
48. K. M. Abraham, *Electrochim. Acta*, **38**, 1233 (1993).
49. K. K. Patel, J. M. Paulsen, and J. Desilvestro, *J. Power Sources*, **122**, 144 (2003).
50. D. Djian, F. Alloin, S. Martinet, H. Lignier, and J. Y. Sanchez, *J. Power Sources*, **172**, 416 (2007).
51. D. S. Eastwood et al., *Adv. Energy Mater.*, **4**, 1 (2014).
52. A. Yermukhambetova et al., *Sci. Rep.*, **6**, 35291 (2016).
53. T. DuBeshter, P. K. Sinha, A. Sakars, G. W. Fly, and J. Jorne, *J. Electrochem. Soc.*, **161**, A599 (2014).
54. T. Osaka, D. Mukoyama, and H. Nara, *J. Electrochem. Soc.*, **162**, A2529 (2015).
55. Z. Deng et al., *J. Electrochem. Soc.*, **160**, A553 (2013).
56. S. Drvarič Talian, J. Moškon, R. Dominko, and M. Gaberšček, *ACS Appl. Mater. Interfaces*, **9**, 29760 (2017).
57. E. Peled et al., *J. Electrochem. Soc.*, **165**, A6051 (2018).
58. V. S. Kolosnitsyn, E. V. Kuzmina, and S. E. Mochalov, *J. Power Sources*, **252**, 28 (2014).
59. N. A. Canas et al., *Electrochim. Acta*, **97**, 42 (2013).
60. S. Risse et al., *J. Power Sources*, **323**, 107 (2016).
61. A. Ganesan, A. Varzi, S. Passerini, and M. M. Shaijumon, *Electrochim. Acta*, **214**, 129 (2016).
62. V. S. Kolosnitsyn, E. V. Kuzmina, E. V. Karaseva, and S. E. Mochalov, *J. Power Sources*, **196**, 1478 (2011).
63. L. Yuan, X. Qiu, L. Chen, and W. Zhu, *J. Power Sources*, **189**, 127 (2009).
64. Y. Li, H. Zhan, S. Liu, K. Huang, and Y. Zhou, *J. Power Sources*, **195**, 2945 (2010).
65. C. Bünzli et al., *J. Electrochem. Soc.*, **162**, A218 (2015).
66. S. Klink et al., *Electrochem. Commun.*, **22**, 120 (2012).
67. M. Ender, A. Weber, and E. Ivers-TiffeÉe, *J. Electrochem. Soc.*, **159**, A128 (2012).
68. J. Zhou and P. H. L. Notten, *J. Electrochem. Soc.*, **151**, A2173 (2004).
69. D. P. Abraham, S. D. Poppen, A. N. Jansen, J. Liu, and D. W. Dees, *Electrochim. Acta*, **49**, 4763 (2004).
70. J. L. Gómez-Cámer and P. Novák, *Electrochem. Commun.*, **34**, 208 (2013).
71. S. Solchenbach, D. Pritzl, E. J. Y. Kong, J. Landesfeind, and H. A. Gasteiger, *J. Electrochem. Soc.*, **163**, A2265 (2016).
72. M. DolleÉ, F. Orsini, A. S. Gozdz, and J.-M. Tarascon, *J. Electrochem. Soc.*, **148**, A851 (2001).
73. R. Petibon et al., *J. Electrochem. Soc.*, **160**, 117 (2013).
74. S. Waluś, A. Robba, R. Bouchet, C. Barchasz, and F. Alloin, *Electrochim. Acta*, **210**, 492 (2016).
75. C. H. Chen, J. Liu, and K. Amine, *J. Power Sources*, **96**, 321 (2001).
76. C. H. Chen, J. Liu, and K. Amine, *Electrochem. Commun.*, **3**, 44 (2001).
77. N. Schweikert, H. Hahn, and S. Indris, *Phys. Chem. Chem. Phys.*, **13**, 6234 (2011).
78. J. C. Burns et al., *J. Electrochem. Soc.*, **158**, A1417 (2011).
79. R. Raccichini, J. W. Dibden, A. Brew, J. R. Owen, and N. García-Aráez, *J. Phys. Chem. B*, **122**, 267 (2018).
80. J. Chen, Y. Yan, T. Sun, Y. Qi, and X. Li, *RSC Adv.*, **4**, 14904 (2014).
81. http://www.toray-bsf.com/en.
82. X. Huang, *J. Solid State Electrochem.*, **15**, 649 (2011).
83. N. P. Bansal and R. H. Doremus, *Handbook of Glass Properties*, Academic Press, (1986).
84. J. M. Elliott and J. R. Owen, *Phys. Chem. Chem. Phys.*, **2**, 5653 (2000).
85. T. F. Esterle, D. Sun, M. R. Roberts, P. N. Bartlett, and J. R. Owen, *Phys. Chem. Chem. Phys.*, **14**, 3872 (2012).
86. C. Martinez-Cisneros, C. Antonelli, B. Levenfeld, A. Varez, and J. Y. Sanchez, *Electrochim. Acta*, **216**, 68 (2016).
87. M. Plaimer et al., *J. Power Sources*, **306**, 702 (2016).
88. K. Prasanna and C. W. Lee, *J. Solid State Electrochem.*, **17**, 1377 (2013).
89. S. M. Al-Mahmoud, J. W. Dibden, J. R. Owen, G. Denuault, and N. Garcia-Araez, *J. Power Sources*, **306**, 323 (2016).
90. R. De Levie, *Electrochim. Acta*, **8**, 751 (1963).
91. R. De Levie, *Electrochim. Acta*, **9**, 1231 (1964).
92. A. Lasia, *Electrochemical Impedance Spectroscopy and its Applications*, Springer, (2014).
93. J. Huang and J. Zhang, *J. Electrochem. Soc.*, **163**, A1983 (2016).
94. C.-F. Chen, A. Mistry, and P. P. Mukherjee, *J. Phys. Chem. C*, **121**, 21206 (2017).
95. S. Malifarge, B. Delobel, and C. Delacourt, *J. Electrochem. Soc.*, **164**, E3329 (2017).
96. M. Gaberscek, J. Moskon, B. Erjavec, R. Dominko, and J. Jamnik, *Electrochem. Solid-State Lett.*, **11**, A170 (2008).
97. S. Dsoke, X. Tian, C. Täubert, S. Schlüter, and M. Wohlfahrt-Mehrens, *J. Power Sources*, **238**, 422 (2013).
98. A. Brew, in *2nd International Conference on Battery & Fuel Cell Technology,* July 27–28 2017, Rome, Italy.
99. Y. Yang, G. Zheng, and Y. Cui, *Chem. Soc. Rev.*, **42**, 3018 (2013).
100. X. Ji and L. F. Nazar, *J. Mater. Chem.*, **20**, 9821 (2010).
101. L. Borchardt, M. Oschatz, and S. Kaskel, *Chem. - A Eur. J.*, **22**, 7324 (2016).
102. Z. W. Seh, Y. Sun, Q. Zhang, and Y. Cui, *Chem. Soc. Rev.*, **45**, 5605 (2016).
103. C. Zu et al., *J. Phys. Chem. Lett.*, **7**, 1392 (2016).
104. T. Zhang, M. Marinescu, S. Walus, P. Kovacik, and G. J. Offer, *J. Electrochem. Soc.*, **165**, A6001 (2018).
105. A. Berger et al., *J. Electrochem. Soc.*, **165**, A1288 (2018).
106. C. N. Lin et al., *J. Power Sources*, **263**, 98 (2014).
107. T. Zhang, M. Marinescu, S. Walus, and G. J. Offer, *Electrochim. Acta*, **219**, 502 (2016).
108. K. A. See et al., *J. Am. Chem. Soc.*, **136**, 16368 (2014).
109. J. W. Dibden, J. W. Smith, N. Zhou, N. Garcia-Araez, and J. R. Owen, *Chem. Commun.*, **52**, 12885 (2016).
110. V. Thangavel et al., *J. Electrochem. Soc.*, **163**, A2817 (2016).